Geomech. Geophys. Geo-energ. Geo-resour.
DOI 10.1007/s40948-017-0051-9

ORIGINAL ARTICLE

Seismicity-permeability coupling in the behavior of gas shales, CO_2 storage and deep geothermal energy

Y. Fang · C. Wang · D. Elsworth · T. Ishibashi

Received: 13 November 2016 / Accepted: 10 January 2017

Abstract Contemporary methods of energy conversions that reduce carbon intensity include sequestering CO_2, fuel switching to lower-carbon sources, such as from gas shales, and recovering deep geothermal energy via EGS. In all of these endeavors, either maintaining the low permeability and integrity of caprocks or in controlling the growth of permeability in initially very-low-permeability shales and geothermal reservoirs represent key desires. At short-timescales of relevance, permeability is driven principally by deformations—in turn resulting from changes in total stresses, fluid pressure or thermal and chemical effects. These deformations may be intrinsically stable or unstable, result in aseismic or seismic deformation, with resulting changes in permeability conditioned by the deformational mode. We report experiments and models to represent the respective roles of mineralogy, texture, scale and overpressures on the evolution of friction, stability and permeability in fractured rocks. Models show a transition from high to low residual coefficient of friction for homogenous mixtures of strong and weak aggregates when the proportion of the weak material reaches 25% with a significant transition occurring at 50%. This transition may occur at much lower proportions where the material is structured, such as in a thin layer. For pre-existing fractures, we observe that fracture permeability declines during shearing while the increased sliding velocity reduces the rate of decline. The physics of these observed behaviors are explored via parametric studies and surface measurement of fractures, showing that both permeability and frictional strength are correlated to the fracture asperity evolution that is controlled in-turn by the sliding velocity and fracture material.

Keywords Induced seismicity · Permeability evolution · Shale gas · CO_2 sequestration · EGS

1 Introduction

The presence of pre-existing faults and fractures in the upper crust (Anderson and Zoback 1982; Curtis 2002) contribute to induced seismicity as a result of fluid injection, in hydraulic fracturing, deep storage of CO_2, and stimulation of EGS reservoirs (Ellsworth 2013; Im et al. 2015; Guglielmi et al. 2015; Majer et al. 2007; McGarr et al. 2002; Shapiro et al. 2006; Walsh and Zoback 2015). In all of these, either maintaining the low permeability and integrity of caprocks or in

Y. Fang · C. Wang · D. Elsworth (✉) · T. Ishibashi
Department of Energy and Mineral Engineering, G3 Center and EMS Energy Institute, Pennsylvania State University, University Park, PA, USA
e-mail: elsworth@psu.edu

T. Ishibashi
Fukushima Renewable Energy Institute, National Institute for Advanced Industrial Science and Technology, Koriyama, Fukushima, Japan

Published online: 20 January 2017

controlling the growth of permeability in initially very-low-permeability shales and geothermal reservoirs are key desires. Hence, it is of particular interest to understand the seismicity-permeability interaction in caprocks and unconventional reservoirs.

Mechanically, the occurrence of induced seismicity depends on the shear strength and the frictional stability of a fault-which in-turn depends on its mineralogical composition (Ikari et al. 2011; Fang et al. 2016). The weakness of natural faults can be explained by the presence of frictionally weak minerals, including talc (Collettini et al. 2009; Moore and Rymer 2007). Early experiments using synthetic mixtures of salts and muscovite/kaolinite (Bos and Spiers 2002; Niemeijer and Spiers 2006) showed that weakening can occur with as low as 10 wt% (weight percentage) of frictionally weak minerals. Shear experiments using mixtures of talc and quartz sand (Carpenter et al. 2009) suggested that 30–50 wt% of frictionally weak minerals were required to weaken the composite gouge—much larger percentages than that observed in some natural weak faults. This difference can be explained by the presence of a structured through-going layer of weak minerals (e.g. talc), which weakens the fault. These observations pose the question of what proportion of frictionally weak minerals are needed, and how thick such a layer need be. Experiments (Moore and Lockner 2011; Niemeijer et al. 2010) suggest that the frictional strength of gouge decreases systematically with an increase in thickness of the talc layer. Additionally, coupled shear-permeability experiments suggest that the permeability evolution of faults is likely linked to such mineralogical properties (Ishibashi et al. 2016).

Permeability is known to change during shear deformation (Elsworth and Goodman 1986). It has been widely observed that failure may occur stably (aseismically) at slow creep rates of long duration (order of 1–100 mm/year) or unstably (seismically) at fast frictional sliding rates of short duration (order of 1 m/s) (Anderson et al. 1996; Brune 1968; Peng and Gomberg 2010; Schmidt et al. 2005). The stability of sliding is governed by the frictional properties of faults and can be described with rate-and-state friction laws (Dieterich 1979a, b; Marone 1998; Ruina 1983; Scholz 1998). These studies provide potential insights into the rheological response of caprocks and unconventional reservoirs with regard to the mode and timing of induced earthquakes. However, it is still unclear whether different styles of permeability evolve from unstable fast sliding of seismic events versus slow-slip aseismic events. In this study, we integrate both experimental and computational methods to (1) explore how fracture permeability changes in response to fracture reactivation; (2) identify hydraulic behavior for different rock types; and (3) probe the relationship between frictional strength with respect to mineralogical composition.

2 Seismicity-permeability observations

In the foregoing it is noted that the friction-permeability relationships are complex and challenging. Thus, we first review assumptions that relax the constraints of real systems and to capture the most fundamental features that reveal the permeability evolution during both aseismic and seismic events via experiments. Then, we will introduce the sample materials, preparation processes and experimental setup and procedures.

2.1 Assumptions and conditions

The experiments explore the relationships between frictional properties and permeability evolution of fractures during shear slip. For the purpose of capturing the most fundamental features, it is necessary to impose the following assumptions:

1. The fracture is assumed to be a parallel plate model following the cubic law. Although this model differs from the natural fractures with complex geometric surfaces, it provides basic insights for fluid flow and solute transport through an individual rock fracture under different stress conditions (Snow 1969). This fracture model also aligns with the underlying assumption of rate and state theory that the fracture geometry is in a regular plane shape (Dieterich 1992).
2. Deionized water, in lieu of aqueous CO_2 fluid, is adopted as the permeant, because the time scale is rapid and flow rate is low, indicating that the minerals at the fractures are not transformed or removed due to reaction or dissolution (Samuelson and Spiers 2012).
3. Slow slip velocities are of more interest and importance than of fast slip. Experimental slip

velocities ranging from $\sim 10^{-1}$ to 10^{1} μm/s are representative of both aseismic slip and seismic slip rate. This assumption is reasonable since abundant observations show that fluid injection induced seismic events can enhance wellbore injectivity and reservoir permeability (Rinaldi et al. 2015; Shapiro and Dinske 2009), suggesting that permeability enhancement due to unstable slip is likely. Furthermore, according to the fracture length-frequency power law (Bonnet et al. 2001), small fractures are distributed in the upper crust and are more likely to be reactivated aseismically with slow slip (Fang et al. 2016). Slow slip can also occur seismically on mis-oriented planes (Kohli and Zoback 2013). Thus it is of more interet to focus on the friction-permeability relationships within the low velocity regime.

4. There is neither thermal cracking nor thermal pressurization during the experiment. This is because the sliding velocity in this experiment is about two orders of magnitude lower than similar experiments (Rice, 2006; Tanikawa et al. 2010, 2014).

The normal stress applied in the experiment is assumed to be equivalent to the in situ effective normal stress that acts on the most favorably orientated fractures after an overpressure is applied. CO_2 reservoir candidates (Allis et al. 2001) are statistically assumed to be located at a depth of ~ 1000 m with average caprock thickness of ~ 110 m, implying that local effective normal stress on the fractures of the overlying caprocks are relatively low.

2.2 Sample material and experimental setup

Low permeability is a necessary attribute for caprock. Most CO_2 sequestration caprock candidates (Allis et al. 2001) form in sedimentary environments near the crustal surface. In this experiment, we select Green River shale as a caprock candidate for reference. The matrix porosity of Green River shale is ~ 0.03 to ~ 0.04 and the permeability is estimated as $\sim 10^{-23}$ m^2 (perpendicular to the bedding) to $\sim 10^{-22}$ m^2 (parallel to the bedding) (Yildirim 2014). The in situ stress field of the Green River formation (Bredehoeft et al. 1976), suggests a strike slip faulting regime near the shallow surface and a normal faulting stress regime below a depth of 200 m, and the maximum horizontal stress σ_H trending along N70W. Stratigraphic analysis indicates that the bottom of the Green River shale formation is at a depth of ~ 950 m (Dyni 2006). Thus, from the measured stress gradient, local in situ stresses are estimated as $\sigma_v = 21.5$, $\sigma_H = 20.0$, $\sigma_h = 14.9$ and $P_0 = 8.8$ MPa respectively. For the experiment, cores with longitudinal lengths of 2 inches and diameters of 1 inch, are drilled and are saw-cut into two halves representing a parallel plate model (Fig. 1a, b). The plate surface is uniformly roughened with grinding powder at a constant rate. The mineralogical composition of the samples is characterized via X-Ray Diffraction analysis, which shows that the samples used in the experiments are dominated by three groups of minerals: carbonate, tectosilicates and phyllosilicates. The experiments are performed within a triaxial testing apparatus that can independently apply confining pressure, pore pressure, and shear velocity and can concurrently monitor the evolution of fracture permeability during the experiments (Fig. 1c).

2.3 Analysis of experimental results

We used the measured data to calculate the frictional strength μ as a function of shear displacement using $\mu = \tau/\sigma_n$. Friction shows a slight decrease after a peak (Fig. 2), being evidence of asperity damage as a progressive removal of the highest asperities from the fracture surface (Fig. 3a). The velocity dependence of friction is interpreted in the framework of rate-state friction (RSF) theory (Dieterich 1979a, b; Marone 1998; Ruina 1983; Scholz 1998) and shows frictional stability or stable sliding. We then evaluate the nonlinear normal stress-dependent aperture (Rutqvist et al. 2008) and apply the cubic law to estimate permeability. To yield a better understanding of the mechanisms of permeability evolution, we model permeability evolution using an analogous parameter to the shear dilation relationship of Samuelson et al. (2009) that is defined as a dilation or compaction parameter $\Delta\phi^i$:

$$\Delta\phi^i = \frac{\Delta b^i_{vel}}{b^{i-1}_{slip}} = \psi^i \cdot \ln\left(\frac{V^{i-1}}{V^i}\left[1 + \left(\frac{V^i}{V^{i-1}} - 1\right) \cdot e^{-V^i \cdot t^i / D^i_c}\right]\right) \quad (1)$$

where Δb^i_{vel} [m] is the aperture change due to the ith velocity change in the slip history; b^{i-1}_{slip} [m] is the

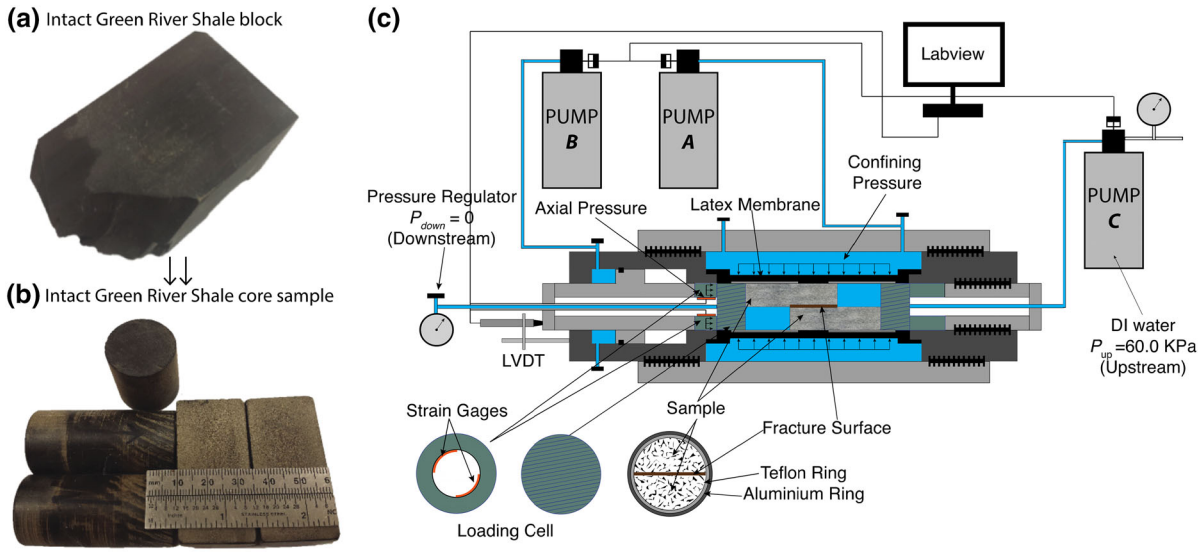

Fig. 1 **a** Natural (intact) Green River Shale block, **b** cored and saw-cut half split of natural GRS, **c** picture of experimental setup for friction-permeability evolution test: Pump A controls the confining pressure (normal stress) applied on the fracture. Pump B controls pressure that provides the source of shear stress applied on the fracture. Pump C injects the fluid at a prescribed flow rate or pressure, allowing the fluid source locates at the origin of the fracture and flow along the fractures

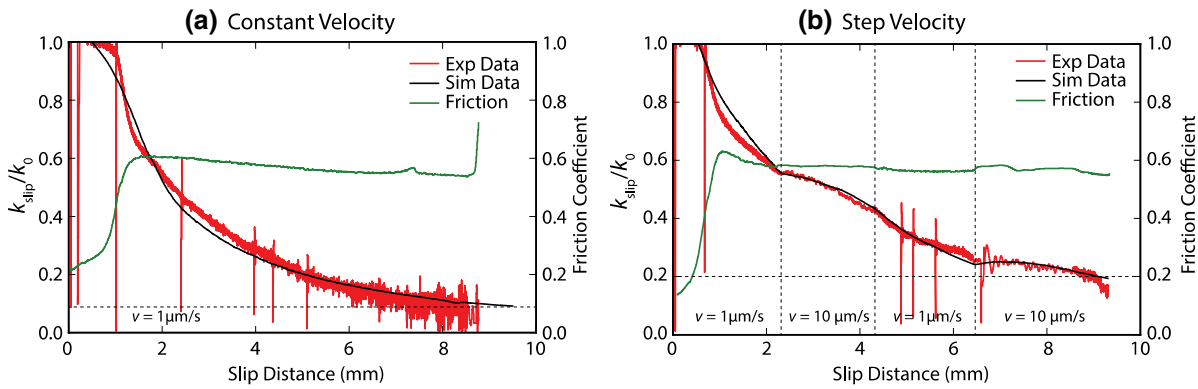

Fig. 2 Relationship between measured friction (*green curve*), measured permeability (*red curve*) and sliding velocity (constant vs. stepped velocity). Simulated permeability is shown in *black*. **a** Scenario of constant slip velocity (1 μm/s), **b** scenario of stepped slip velocity (1, 10, 1, 10 μm/s)

aperture before the shear velocity is changed; ψ^{i} is a compaction/dilation factor that pertains to the fracture material and attributes; t^{i} [s] is the time since the ith velocity step from V^{i-1} to V^{i}. Hence, the modelled fracture aperture b_{evo} [m] that evolves during shear slip and the corresponding permeability k_{f} [m^2] are expressed as,

$$b_{evo} = b_{slip}^{i-1} \cdot \left(1 + \Delta\phi^{i}\right) \tag{2}$$

$$k_f = \frac{b_{evo}^2}{12} \tag{3}$$

The measured permeability, illustrated in red in Fig. 2, declines exponentially at a constant sliding velocity. As a comparison in Fig. 2b, although a similar declining trend of the measured permeability is observed, the change in sliding velocity from 1 to 10 μm/s clearly slows down the rate of decrease of the permeability—while the sliding velocity drops from 10 to 1 μm/s, the rate of decrease accelerates. Clearly, the slope of the decrease in permeability asymptotes after a shear slip of 6–8 mm, suggesting that the asperity height distribution experiences a relatively

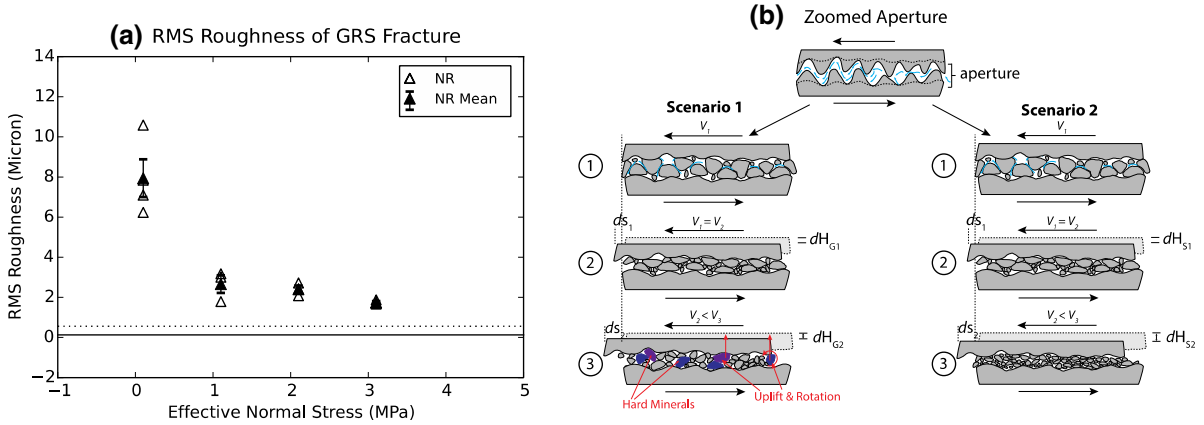

Fig. 3 **a** Root mean square (RMS) roughness of planar fracture surface of a split core of Green River Shale. Plots with normal stress at 0 refer to the initial asperity before shear sliding. Plots with normal stress at 1–3 MPa refer to the asperity after shear sliding (NR stands for the natural intact rocks). **b** Conceptual model of permeability evolution. Scenario 1: Brittle-like material that is composed of hard minerals. During shearing, the hard minerals are difficult to comminute into small particles and the fracture may dilate significantly. Scenario 2: Ductile material that is composed of soft minerals. When subject to shearing, the soft minerals readily deform and comminute into smaller particles and fill the void

small change. It is noteworthy that the eventual permeability during velocity stepping is enhanced by ∼10% compared to that at constant velocity, suggesting that the high sliding velocity may, to some extent, enhance the fracture permeability. The modelled permeability matches well with the measured permeability for both constant velocity and stepped-velocity sliding. These results may be interpreted by physical processes as follows: (1) within the slow slip velocity domain, permeability always declines as shear slip increases due to the reduction of asperity height up to the time that a steady state of asperity height is reached; (2) changing the sliding velocity may enhance or diminish the changing rate of permeability via dilation or compacting the generated wear products as illustrated in Fig. 3b. In regard to frictional evolution, the frictional strength stabilized within the range ∼0.57 to ∼0.59 at a slip distance of ∼8 mm. A slight velocity strengthening is observed from Fig. 2b when the sliding velocity step is applied.

2.4 Summary of experimental results and discussion

The experimental results suggest that the friction-permeability relationship can be linked via the dynamic evolution of asperities and contact state of fracture surfaces. It is speculated that the deformation of the generated wear products may result in the dilation or compaction of the fracture and eventually alter the fracture hydraulic conductivity. We speculate that this linkage is a function of the attributes of the fracture material, particularly the mineral compositions and fracture roughness and their micromechanical properties. These effects of material attributes are explored in the following numerical modelling.

3 Friction-stability modelling

3.1 Numerical method

The mechanical response of faults may be explored using numerical models. The Distinct Element Method (Cundall and Strack 1979) is based on the dynamic interaction of distinct grains and has been successfully applied to varies geophysical research fields, for example, investigating the effect of particle size distribution and inter-particle friction on the deformation mechanisms of granular fault zones (Morgan and Boettcher 1999) and experiments (Abe and Mair 2005, 2009). Here we explore the application of a DEM model in simulating the shear strength evolution of fault gouges consisting of homogeneous and heterogeneous mixtures of a frictionally strong phase and a frictionally weak phase. Simulations of direct shear experiments show promising results that match the previous observations from biaxial direct shear experiments.

A DEM model has been developed using Particle Flow Code 2D (PFC2D, ITASCA Consulting Group). The geometry of the DEM model is a scaled duplication of the configuration of a biaxial direct shear test (Mair and Marone 1999), in which the gouge sample is confined between saw-tooth grooved platens. The numerical model consists of two saw-tooth-grooved shear platens and simulated fault gouge represented by circular particles sandwiched between the platens (shown as Fig. 4). The size of the assembly is 20 mm in length and approximately 2.5 mm in width (after compaction, small variations may occur due to different sample parameters). Wall boundaries are added outside the shear platens with adjustable velocities. Stable confining stress can be maintained during the experiment by continuously adjusting the velocity of the wall boundary. Mixed frictionally strong and frictionally weak phases are represented by circular particles with different size and properties. The radii for particles in the assembly range from 250 to 500 μ for the frictionally strong phase and 200–250 μ for the weak phase. The particle sizes follow a Gaussian distribution. The numerical tests were conducted through the following steps: (1) generate shear platens and wall boundaries; (2) generate loosely distributed particles between two shear platens; (3) apply controlled velocity on both shear platens to compact loose particles until reaching a desired confining stress, adjusting velocity applied to wall boundaries to maintain the confining stress; (4) actuate one shear plate with a prescribed velocity while holding the other platen static.

A linear-elastic contact model is implemented between gouge particles in the model, which consists of two sets (normal direction and shear direction) of parallel aligned springs and dashpots. A slider is applied in the shear direction to simulate sliding behaviour according to Coulomb friction. In order to mitigate the strong rolling tendency (Morgan and McGovern 2005; Morgan 2004) of circular shaped particles, lacking the influence of three-dimensional particle inter-locking effects, rotation is restricted in all simulations.

3.2 Model configuration

3.2.1 Homogeneous mixtures

The model configuration for homogeneous mineral mixtures is shown in Fig. 4a. The proportion of the frictionally weak phase is varied from 0 to 100 wt% with an interval of 25 wt%. The inter-particle coefficient of friction is 0.60 for frictionally strong particles and 0.10 for frictionally weak particles respectively.

3.2.2 Heterogeneous mixtures

The model configuration for heterogeneous mineral mixtures is shown in Fig. 4b. Different from the homogeneous mixture, a through-going layer of

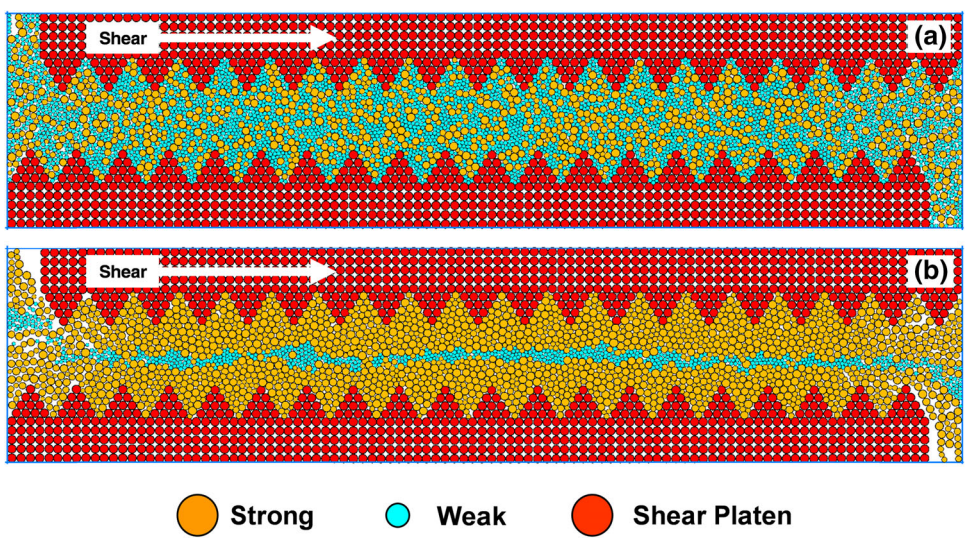

Fig. 4 DEM model configuration: **a** homogeneous mixtures, **b** heterogeneous mixtures

frictionally weak particles is sandwiched by a frictionally strong mineral matrix. The relative thickness (i.e. the effective thickness ratio of the frictionally weak mineral layer and the gouge mixture) of the through-going weak layer is varied in an ascending order. Specifically, relative layer thickness of 0.05, 0.10, 0.25, and 0.50 are considered in this study. Bulk shear strength data obtained from two numerical runs of pure frictionally weak and strong mineral are considered as reference cases (i.e. relative weak layer thickness of 0.00/1.00).

3.3 Effect of mineralogical composition on shear strength of fault gouge

The bulk shear strength can be represented by the friction coefficient of the system. Evolution of friction coefficient are plotted against shear displacement in Fig. 5a. It is clearly observed that the bulk coefficient of friction decreases as the weight percentage of the frictionally weak mineral increases. To be specific, the residual friction coefficient is ~0.60 with 0 wt% frictionally weak materials. The residual coefficient of friction reduces from ~0.60 to ~0.33 with 25 wt% frictionally weak materials present, showing a large reduction in shear strength. Furthermore, the reduction in shear strength slows if more frictionally weak minerals are introduced (i.e. 50, 75 wt%). When frictionally weak mineral exceeds 75 wt%, the residual coefficient of friction exhibits similar magnitude to that of the gouge sample consisting of pure frictionally weak minerals. The transitional behavior of decreasing in residual coefficient of friction is plotted as Fig. 5b. This trend from the simulations matches previous experimental observations (Carpenter et al. 2009; Moore and Lockner 2011).

3.4 Effect of mineralogical heterogeneity on shear strength of fault gouge

Similarly, heterogeneous mixtures are simulated using the model configuration. The relative width of the frictionally weak layer is altered in each numerical run to investigate its effect on the reduction in the bulk friction coefficient. The gouge samples are confined and sheared in the same manner as the homogeneous cases. The evolution of friction coefficient of each numerical run is shown in Fig. 6a. It can be clearly observed that bulk friction coefficient decreases as the relative width of the frictionally weak layer increases. In particular, the bulk residual coefficient of friction drops from ~0.60 to ~0.40 with an increase in relative layer thickness from 0.00 to 0.05 (Fig. 6b). It is also apparent that for a weak layer relative thickness of 0.05, the weak layer is split into small clusters by the bridging of frictionally strong mineral particles. Thus it is not able to form a continuous through-going zone of localization. However, even these non-continuous "weak zones" can induce a large reduction of the bulk friction coefficient.

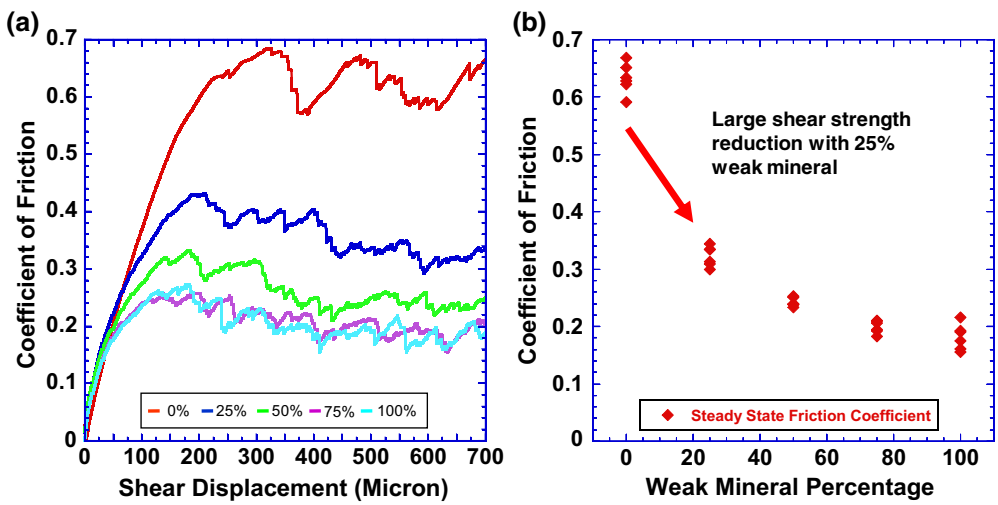

Fig. 5 Simulation results of homogeneous mixtures of frictionally weak and strong minerals: **a** evolution of coefficient of friction, **b** steady state friction coefficient at against weak mineral weight percentage

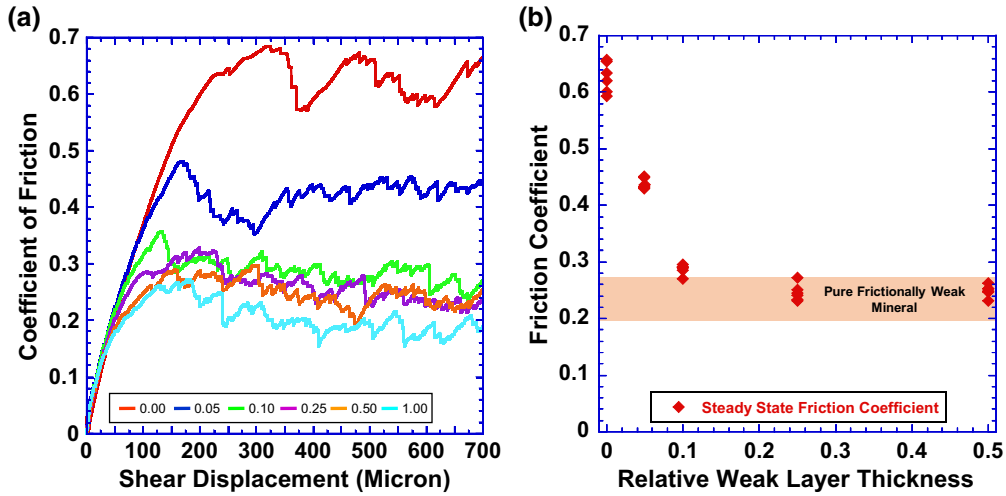

Fig. 6 Results for the simulation of heterogeneous mixtures of frictionally weak and strong minerals: **a** evolution of coefficient of friction, **b** steady state friction coefficient versus relative thickness of frictionally weak layer

At a relative layer thickness of 0.10, the residual coefficient of friction of the gouge is reduced to ~0.26 at steady state, which is close to the residual coefficient of friction of pure, frictionally weak, mineral (~0.22). This suggests that a relative thickness of 0.1 is sufficient for the frictionally weak minerals to form a continuous localized zone during slip, forcing shear to be localized on the weak zone, showing the dominance of the frictionally weak mineral. Similar bulk residual friction coefficients are also observed with a relative thicknesses of 0.25 and of 0.50. This trend is consistent with experimental observations (Niemeijer et al. 2010).

3.5 Summary of numerical simulation results and discussion

A DEM model of direct-shear tests on fault gouge samples is constructed to simulate the shear strength evolution of faults. Gouge samples consist of homogeneous mixtures of frictionally strong minerals and frictionally weak minerals with prescribed compositions. Similarly, heterogeneous mixtures consist of a though-going frictionally weak mineral layer sandwiched in a frictionally strong mineral matrix are tested with prescribed relative weak layer thickness. Observations of the onset of the strong weakening effect match with previous experimental observations. Relatively small amount of frictionally weak minerals present in the system can result in a significant reduction in bulk shear strength. Thus, modelling results support the argument that the shear strength of faults depends strongly on mineralogical composition and texture, illustrating the applicability of DEM modelling in simulating the shear strength evolution in complex faults.

4 Conclusions

The following conclusions can be drawn from the observations:

1. Seismicity-permeability relationships can be linked via the dynamic evolution of asperities and contact state of fracture surfaces in which the mineralogical composition defines the mode of seismicity and control the mechanical strength of fracture asperities that eventually affect permeability evolution.
2. In homogenous mixtures, the residual shear strength of the gouge sample can be reduced by ~50 % (~0.6 to ~0.3) with 25 wt% frictionally weak mineral present in the gouge.
3. Homogenous gouge samples containing more than 25 wt% of frictionally weak minerals exhibit similar residual coefficient of friction as pure frictionally weak minerals, showing the dominant influence of the frictionally weak minerals.
4. In heterogeneous mixtures, a frictionally weak layer can reduce the residual coefficient of friction

by ~30% (~0.6 to ~0.4) with a relative weak layer thickness of only 0.05. Furthermore, relative weak layer thickness greater than 0.10 can reduce the residual coefficient of friction to a magnitude of pure frictionally weak mineral.

Acknowledgements This work is the result of support provided by DOE Grant DE-FE0023354. This support is gratefully acknowledged.

References

Abe S, Mair K (2005) Grain fracture in 3D numerical simulations of granular shear. Geophys Res Lett 32(5):1–4. doi:10.1029/2004GL022123

Abe S, Mair K (2009) Effects of gouge fragment shape on fault friction: new 3D modelling results. Geophys Res Lett 36(23):2–5. doi:10.1029/2009GL040684

Allis R, Chidsey T, Gwynn W, Morgan C, White S, Adams M, Moore J (2001) Natural CO2 reservoirs on the Colorado Plateau and southern Rocky Mountains: candidates for CO2 sequestration. In: Proceedings of the first national conference on carbon sequestration. pp 14–17

Anderson RN, Zoback MD (1982) Permeability, underpressures, and convection in the oceanic crust near the Costa Rica Rift, eastern equatorial Pacific. J Geophys Res 87(B4):2860. doi:10.1029/JB087iB04p02860

Anderson JG, Wesnousky SG, Stirling MW (1996) Earthquake size as a function of fault slip rate. Bull Seismol Soc Am 86(3):683–690

Bonnet E, Bour O, Odling NE, Davy P, Main I, Cowie P, Berkowitz B (2001) Scaling of fracture system in geological media. Rev Geophys 39(3):347–383

Bos B, Spiers CJ (2002) Frictional-viscous flow of phyllosilicate-bearing fault rock: microphysical model and implications for crustal strength profiles. J Geophys Res 107(B2):2028. doi:10.1029/2001JB000301

Bredehoeft JD, Wolff RG, Keys WS, Shuter E (1976) Hydraulic fracturing to determine the regional in situ stress field, Piceance Basin, Colorado. Bull Geolog Soc Am 87(2):250–258. doi:10.1130/0016-7606(1976)87<250:HFTDTR>2.0.CO;2

Brune JN (1968) Seismic moment, seismicity, and rate of slip along major fault zones. J Geophys Res 73(2):777–784

Carpenter BM, Marone C, Saffer DM (2009) Frictional behavior of materials in the 3D SAFOD volume. Geophys Res Lett 36(5):1–5. doi:10.1029/2008GL036660

Collettini C, Niemeijer A, Viti C, Marone C (2009) Fault zone fabric and fault weakness. Nature 462(7275):907–910. doi:10.1038/nature08585

Cundall PA, Strack ODL (1979) A discrete numerical model for granular assemblies. Géotechnique. doi:10.1680/geot.1979.29.1.47

Curtis JB (2002) Fractured shale-gas systems. AAPG Bull 11(11):1921–1938. doi:10.1306/61EEDDBE-173E-11D7-8645000102C1865D

Dieterich JH (1979a) Modeling of rock friction 1. Experimental results and constitutive equations. J Geophys Res Solid Earth 84(B5):2161–2168. doi:10.1029/JB084iB05p02161

Dieterich JH (1979b) Modeling of rock friction: 1. Experimental results and constituve equations. J Geophys Res 84(9):2161–2168. doi:10.1007/BF00876539

Dieterich JH (1992) Earthquake nucleation on faults with rate- and state-dependent friction. Tectonophysics 211(1):115–134. doi:10.1016/0040-1951(92)90055-B

Dyni JR (2006) Geology and resources of some world oil-shale deposits. US Department of The Interior, US Geological Survey

Ellsworth W (2013) Injection-induced earthquakes. Science 341(6142):142–149. doi:10.1126/science.1225942

Elsworth D, Goodman RE (1986) Characterization of rock fissure hydraulic conductivity using idealized wall roughness profiles. Int J Rock Mech Min Sci Geomech Abstr 23(3):233–243. doi:10.1016/0148-9062(86)90969-1

Fang Y, den Hartog SAM, Elsworth D, Marone C, Cladouhos T (2016) Anomalous distribution of microearthquakes in the Newberry Geothermal Reservoir: mechanisms and implications. Geothermics 63:62–73. doi:10.1016/j.geothermics.2015.04.005

Guglielmi Y, Cappa F, Avouac J, Henry P, Elsworth D (2015) Seismicity triggered by fluid injection-induced aseismic slip. Science 348(6240):1224–1227. doi:10.1126/science.aab0476

Ikari MJ, Niemeijer AR, Marone C (2011) The role of fault zone fabric and lithification state on frictional strength, constitutive behavior, and deformation microstructure. J Geophys Res Solid Earth 116(8):1–25. doi:10.1029/2011JB008264

Im K, Elsworth D, Guglielmi YG, Mattioli GS (2015) Use of geodesy to discriminate deformation mechanics in geothermal reservoirs. American Rock Mechanics Association

Ishibashi T, Asanuma H, Fang Y, Wang C, Elsworth D (2016) Exploring the link between permeability and strength evolution during fracture shearing. American Rock Mechanics Association

Kohli AH, Zoback MD (2013) Frictional properties of shale reservoir rocks. J Geophys Res Solid Earth 118(9):5109–5125. doi:10.1002/jgrb.50346

Mair K, Marone C (1999) Friction of simulated fault gouge for a wide range of velocities and normal stresses. J Geophys Res 104(B12):28899–28914

Majer EL, Baria R, Stark M, Oates S, Bommer J, Smith B, Asanuma H (2007) Induced seismicity associated with enhanced geothermal systems. Geothermics 36(3):185–222. doi:10.1016/j.geothermics.2007.03.003

Marone C (1998) Laboratory-derived friction laws and their application to seismic faulting. Ann Rev Earth Planet Sci 26:643–696. doi:10.1146/annurev.earth.26.1.643

McGarr A, Simpson D, Seeber L (2002) Case histories of induced and triggered seismicity. Int Geophys 81:647–661. doi:10.1016/S0074-6142(02)80243-1

Moore DE, Lockner DA (2011) Frictional strengths of talc-serpentine and talc-quartz mixtures. J Geophys Res Solid Earth 116(B01403):1–17. doi:10.1029/2010JB007881

Moore DE, Rymer MJ (2007) Talc-bearing serpentinite and the creeping section of the San Andreas fault. Nature 448(7155):795–797. doi:10.1038/nature06064

Morgan JK (2004) Particle dynamics simulations of rate- and state-dependent frictional sliding of granular fault gouge. Pure appl Geophys 161(9–10):1877–1891. doi:10.1007/s00024-004-2537-y

Morgan JK, Boettcher MS (1999) Numerical simulations of granular shear zones using the distinct element method: 1. Shear zone kinematics and the micromechanics of localization. J Geophys Res 104(B2):2703–2719. doi:10.1029/1998JB900056

Morgan JK, McGovern PJ (2005) Discrete element simulations of gravitational volcanic deformation: 1. Deformation structures and geometries. J Geophys Res B Solid Earth 110(5):1–22. doi:10.1029/2004JB003252

Niemeijer AR, Spiers CJ (2006) Velocity dependence of strength and healing behaviour in simulated phyllosilicate-bearing fault gouge. Tectonophysics 427(1–4):231–253. doi:10.1016/j.tecto.2006.03.048

Niemeijer A, Marone C, Elsworth D (2010) Fabric induced weakness of tectonic faults. Geophys Res Lett 37(3):1–5. doi:10.1029/2009GL041689

Peng Z, Gomberg J (2010) An integrated perspective of the continuum between earthquakes and slow-slip phenomena. Nat Geosci 3(9):599–607. doi:10.1038/ngeo940

Rice JR (2006) Heating and weakening of faults during earthquake slip. J Geophys Res Solid Earth 111(B05311):1–29. doi:10.1029/2005JB004006

Rinaldi AP, Rutqvist J, Sonnenthal EL, Cladouhos TT (2015) Coupled THM modeling of hydroshearing stimulation in tight fractured volcanic rock. Transp Porous Media 108:131–150. doi:10.1007/s11242-014-0296-5

Ruina A (1983) Slip instability and state variable friction law. J Geophys Res. doi:10.1029/JB088iB12p10359

Rutqvist J, Freifeld B, Min KB, Elsworth D, Tsang Y (2008) Analysis of thermally induced changes in fractured rock permeability during 8 years of heating and cooling at the Yucca Mountain Drift Scale Test. Int J Rock Mech Min Sci 45(8):1373–1389. doi:10.1016/j.ijrmms.2008.01.016

Samuelson J, Spiers CJ (2012) Fault friction and slip stability not affected by CO_2 storage: evidence from short-term laboratory experiments on North Sea reservoir sandstones and caprocks. Int J Greenh Gas Control 11:78–90. doi:10.1016/j.ijggc.2012.09.018

Samuelson J, Elsworth D, Marone C (2009) Shear-induced dilatancy of fluid-saturated faults: experiment and theory. J Geophys Res Solid Earth 114(12):1–15. doi:10.1029/2008JB006273

Schmidt DA, Bürgmann R, Nadeau RM, D'Alessio M (2005) Distribution of aseismic slip rate on the Hayward fault inferred from seismic and geodetic data. J Geophys Res B Solid Earth 110(B08406):1–15. doi:10.1029/2004JB003397

Scholz CH (1998) Earthquakes and friction laws. Nature 391(6662):37–42. doi:10.1038/34097

Shapiro SA, Dinske C (2009) Fluid-induced seismicity: pressure diffusion and hydraulic fracturing. Geophys Prospect 57(2):301–310. doi:10.1111/j.1365-2478.2008.00770.x

Shapiro SA, Dinske C, Rothert E (2006) Hydraulic-fracturing controlled dynamics of microseismic clouds. Geophys Res Lett 33(L14312):1–5. doi:10.1029/2006GL026365

Snow DT (1969) Anisotropic permeability of fractured media. Water Resour Res 5(6):1273–1289. doi:10.1029/WR005i006p01273

Tanikawa W, Sakaguchi M, Tadai O, Hirose T (2010) Influence of fault slip rate on shear-induced permeability. J Geophys Res Solid Earth 115(B07412):1–18. doi:10.1029/2009JB007013

Tanikawa W, Tadai O, Mukoyoshi H (2014) Permeability changes in simulated granite faults during and after frictional sliding. Geofluids 14:481–494. doi:10.1111/gfl.12091

Walsh FR, Zoback MD (2015) Oklahoma's recent earthquakes and saltwater disposal. Sci Adv. doi:10.1126/sciadv.1500195

Yildirim LTO (2014) Evaluation of petrophysical properties of gas shale and their change due to interaction with water. Master Thesis, The Pennsylvania State University